2018

# Raman studies on silicene and germanene

Yani Liu
*University of Wollongong*

Jincheng Zhuang
*University of Wollongong*, jz673@uowmail.edu.au

Weichang Hao
*Beihang University*, whao@buaa.edu.cn

Yi Du
*University of Wollongong*, ydu@uow.edu.au

## Publication Details

Liu, Y., Zhuang, J., Hao, W. & Du, Y. (2018). Raman studies on silicene and Germanene. Surface Innovations, 6 (1-2), 4-12.

# Raman studies on silicene and germanene

**Abstract**
Two-dimensional (2D) group IV elemental materials are expected to have similar electronic features to their lightest analogue, graphene. The favorable hybridization state of heavier group IV elements is the sp 3 state, leading to buckled structures instead of a planar one. These buckled structures could modulate the vibrational properties of these 2D materials by introducing a strain effect. In this review, the authors focus on the recent research on the Raman spectra of silicene and Germanene from both the theoretical and experimental sides. The abundant superstructures of silicene and Germanene are formed due to the different interaction strengths between silicene/germanene and underlying substrate, providing a way to modulate their phonon vibrational properties. Several factors affecting the vibrational modes are discussed, including the strain, doping, coverage and defect effects. Furthermore, the relationship between electron-phonon coupling strength and these factors is established based on the variation of Raman peak position and linewidth. Finally, the authors provide an overview of the general outlook and challenges for this field.

**Disciplines**
Engineering | Physical Sciences and Mathematics

**Publication Details**
Liu, Y., Zhuang, J., Hao, W. & Du, Y. (2018). Raman studies on silicene and Germanene. Surface Innovations, 6 (1-2), 4-12.

# Raman Studies on Silicene and Germanene

Yani Liu,[1,2,3] Jincheng Zhuang,[1] Weichang Hao,*[2,3] Yi Du*[1,3]

[1]Institute for Superconducting and Electronic Materials (ISEM), University of Wollongong, Wollongong, NSW 2525, Australia

[2]Department of Physics and Key Laboratory of Micro-Nano Measurement, Manipulation and Physics, Ministry of Education, Beihang University, Beijing 100191, China

[3]BUAA-UOW Joint Research Centre, Beihang University, Beijing 100191, China

*Corresponding author e-mail address: yi_du@uow.edu.au and whao@buaa.edu.cn

**Key Words:** Raman spectroscopy, Scanning tunnelling microscopy, Thin film

## Abstract

Two dimensional (2D) group IV elemental materials are expected to have similar electronic features to their lightest analogue, graphene. The favorable hybridization state of heavier group IV elements is the $sp^3$ state, leading to buckled structures instead of a planar one. These buckled structures could modulate the vibrational properties of these 2D materials by introducing a strain effect. In this review, we focus on the recent research on the Raman spectra of silicene and germanene from both the theoretical and experimental sides. Several factors affecting the vibrational modes are discussed, including the strain, doping, coverage, and defect effects. Finally, we provide an overview of the general outlook and challenges for this field.

## Introduction

Graphene, an ideal two-dimensional (2D) material with a honeycomb lattice, has evoked tremendous interests since it was first isolated in 2004, as it is the building block of other carbon allotropes. Its chemical stability, ballistic transport at room temperature, and linear energy-momentum dispersion make it a promising candidate for nanoelectronic applications, especially for high-frequency and low-consumption field-effect transistors (FETs).[1] The most widely used and powerful identification and characterization tool for graphene is Raman spectroscopy, which promises unambiguous, high-throughput, and nondestructive identification.[2] The Raman results provide not only the phonon vibrational information, but also information on the electronic features through the electron-phonon coupling (EPC).[3-5] The internal/external factors, such as defects, doping, strain, varied layer numbers, and electric/magnetic fields, modulate the electronic structure of graphene and further affect the positions, intensities, and widths of the Raman peaks.[5-18] Thus, all these observed effects could be better understood after careful and comprehensive interpretation of the Raman spectrum. In fact, the two inequivalent carbon atoms per unit cell of graphene contribute six normal modes at the Brillouin zone center Γ: $A_{2u}$ (one degenerate out-of-plane acoustic mode) + $B_{2g}$ (one degenerate out-of-plane optical mode) + $E_{1u}$ (two degenerate in-plane acoustic mode) + $E_{2g}$ (two degenerate in-plane optical mode), as shown in Figure 1. The typical G peak located at ~1580 $cm^{-1}$ corresponds to the Raman active $E_{2g}$ phonon at the Γ point.[2] Its position shows a monotonic trend with increased carrier doping due to the increased onset energy of G band decay into electron-hole pairs.[10] The peak located at ~1350 $cm^{-1}$ is correlated with the breathing $A_{1g}$ modes of six-atom rings, and comes from transverse optical (TO) phonons around the Brillouin zone corner K,[19] as displayed in Figure 1. This so-called D peak requires the non-zero phonon wave vector to be activated by the defects, and thus shows a strong

dependence on the defect densities.[20] In addition, the double resonance corresponding to the $A_{1g}$ mode is an intervalley process connecting two different cones around K and K′, leading to the stronger/weaker D peak at the armchair/zigzag edge, respectively, and providing criteria to determine the charity nature of the different edges.[21,22] In addition, the low frequency $E_{2g}$ mode located at ~42 $cm^{-1}$ is related to the interlayer motions and provides criteria for the determination of the layer numbers.[23]

The other group IV elemental 2D materials, silicene and germanene, were first studied by theoretical predictions due to the absence of their layered bulk allotropes. Unlike the planar honeycomb network of $sp^2$ hybridized carbon atoms in graphene, the atomic arrangements of these 2D materials are mostly buckled/puckered hexagonal structures due to the varied interatomic distances.[24,25] The buckled structure could weaken the lateral overlapping of $p_z$ orbitals, resulting in mixed $sp^2/sp^3$ hybridized states. The simulated electronic structures show a tunable energy gap in addition to the Dirac cone for these novel 2D materials due to the enhanced spin-orbit coupling strength, leading to the possible realization of a quantum spin Hall effect (QSHE) at room temperature.[24] Recently, silicene and germanene have been successfully synthesized by using molecular beam epitaxy (MBE) with support of underlying substrate.[26,27] The interaction between the 2D materials and the substrate plays a crucial role in stabilizing the special 2D structures, and determines the buckled structures and correlated electronic properties, contributing to the abundant vibrational modes among the varied superstructures.

This review focuses on the Raman studies of the recently explored group IV elemental 2D materials, silicene and germanene, from both the theoretical and the experimental points of view. The effects of strain, doping, coverage, and defect effects on the Raman spectrum are comprehensively discussed. Meanwhile, the relationship between the EPC and Dirac fermions is

illustrated through Raman scattering, which provides a direct route to investigate the exotic properties of these buckled two-dimensional honeycomb materials.

**Silicene**

Silicene is expected to have similar electronic features to its lightest analogue graphene, and the Dirac cones are located at the K and K′ points of the silicene Brillouin zone (BZ). The calculated free-standing (FS) silicene shows a honeycomb geometry with the silicon atoms alternatively buckled down and up, as shown in Figure 2(a), where the degree of buckling is around 0.44 Å and the bond length is 2.28 Å.[24] The simulation results show the characteristic $E_{2g}$ peak is located at around 570 $cm^{-1}$ (Figure 2(b)).[28,29] This value is much larger than that in bulk Si(111) (~520 $cm^{-1}$),[30] which may have resulted from significant variation of the silicon bond length between FS silicene and silicon. In fact, the long-wavelength optical phonon $E_{2g}$ mode in silicene is predicted to be strictly dependent on the Si-Si bond length as well as the buckling height, *i.e.*, the frequency of the $E_{2g}$ peak decreases as the degree of buckling and bond length increase.[31] Experimentally, silicene has been successfully grown on Ag(111),[26,32-39] Ir(111),[40] Ru(0001),[41] $ZrB_2$(00001),[42] $MoS_2$,[43] and *h*-$MoSi_2$ substrates,[44] and has been formed in the intercalation compound $CaSi_2$.[5] The most commonly used substrate for the fabrication of silicene is Ag(111), in which the abundant superstructures are identified by varying the silicon coverage and substrate temperature.[32] The mixed phase, $\sqrt{13}\times\sqrt{13}/4\times4$ with respect to $1\times1$ Ag (111), is formed in the first layer of the silicon nanosheet, as shown in Figure 3(a) and (b). The atomic structural modes of these two phases are plotted in Figure 3(d) and (e), where only one out of fourteen silicon atoms occupies the highest plane for $\sqrt{13}\times\sqrt{13}$ phase, while there are six out of eighteen silicon atoms buckled up for $4\times4$ phase. *Ex-situ* Raman measurements were first performed on this mixed phase after covering it with an $Al_2O_3$ capping layer at room temperature.[46] Based on the density functional

theory (DFT) calculations for each superstructure, the first-order asymmetric peak located at 516 $cm^{-1}$ is interpreted as the zone-centre $E_{2g}$ vibrational mode, corresponding to the bond stretching of all $sp^2$ silicon atoms. It shifts to a lower wavenumber compared with FS silicene due to the tensile strain originating from the buckling structure. The broad and asymmetric shoulder located at 440-500 $cm^{-1}$ is attributed to the $A_{1g}$ mode activated by the intrinsic substrate-induced disorder. Comprehensive information on the samples may not be completely reflected, however, due to the possible oxidization and strong influence of the capping layer during the *ex-situ* measurements. The details of the phonon modes and their relationship to the silicene electronic properties are still unclear. Thus, an *in-situ* Raman study on silicene under ultrahigh vacuum (UHV) is highly desirable for identifying silicene in different phases and revealing the origins of its exotic properties.

*In situ* Raman spectroscopy on silicene layers epitaxially grown on Ag(111) surfaces with different phases was first conducted by Zhuang *et al*.[47] The $E_{2g}$ peak is at 530 $cm^{-1}$ for the mixed phase measured at 77 K. The obvious blue-shift of the $E_{2g}$ peak frequency in the mixed phase compared to that in Si(111), as shown in Figure 4(a), is solid evidence for distinguishing the silicene layers from the building blocks of bulk Si(111) crystal. The shoulder peak from 495 $cm^{-1}$ to 508 $cm^{-1}$ is most likely attributable to a quantum confinement effect similar to those in microcrystalline silicon and silicon nanowires.[48,49] Similar results have also been reported by Díaz Álvarez *et al*,[50] indicating that the silicene orbitals rather behave as distorted $sp^3$ hybrid orbitals. Furthermore, the peak at 230 $cm^{-1}$ shows a strong polarization direction and is correlated with the out-of-plane displacement of Si-atoms, a vibrational mode that is supported by the buckling.[51,52] The blue-shift of the $E_{2g}$ peak and the presence of the out-of-plane optical mode can be explained by the strong interaction between the Si adlayer and underlying Ag(111) substrate. Such a significant interaction is consistent with the angle-resolved photoemission spectroscopy (ARPES) measurements, where a

hybrid surface metallic state is formed by the first layer silicene and the Ag(111), leading to the absence of Dirac fermion characteristics.[37,53,54]

Another superstructure, √3×√3 phase in terms of 1×1 FS silicene, is present from the second layer, in which two out of six atoms are buckled up in one unit cell (Figure 3(c) and (f)). It is noticeable that a quasiparticle interference (QPI) pattern and Dirac cones have been detected by scanning tunnelling spectroscopy (STS) and ARPES measurements, respectively.[33,34,47,55-57] Thus, the √3×√3 phase is closest to the FS silicene and preserves the Dirac fermion characteristics, which may be due to its low degree of buckling.[58] Interestingly, the intensity of the $E_{2g}$ mode peak in √3×√3 phase is significantly enhanced compared to that in √13×√13/4×4 mixed phase, as shown in Figure 4(b). Since the $E_{2g}$ vibrational mode corresponds to the bond stretching of all $sp^2$ silicon atoms, the higher $E_{2g}$ peak intensity implies that the $sp^2$ state is a more dominant component in √3×√3 phase, which agrees well with the structural and electronic properties of √3×√3 phase measured by scanning tunnelling microscopy (STM) and ARPES, as discussed above. Nevertheless, the $E_{2g}$ peak position (526 $cm^{-1}$ to 530 $cm^{-1}$) is far away from that of its FS counterpart (~570 $cm^{-1}$) (Figure 4(c)). There are two factors contributing to the $E_{2g}$ peak shift. One is the tensile strain effect evoked by lattice mismatch between the silicene and the substrate, leading to the redshift in the peak frequency.[47] The average Si-Si bond length in the √3×√3 superstructure is around 2.35 Å, giving a tensile strain of 5% compared to that of FS silicene (~2.24 Å), which softens the peak position of $E_{2g}$ mode from 570$cm^{-1}$ (FS silicene) to 530$cm^{-1}$ (low-buckled silicene). The other one is the electron doping effect from the underlying Ag(111) substrate, which is verified by the ARPES results, with the Dirac point located at around 0.3 eV below the Fermi level.[34,47,56] The Fermi energy level determines the onset energy of virtual electron-hole pairs that renormalize the $E_{2g}$ phonon energy.[10] It should be noted that the $E_{2g}$ could be defined as a characteristic phonon mode in EPC

matrix elements, and could be applied to evaluate the EPC strength which is determined by electron density of states and the mean electron-phonon coupling potential at the Fermi level.[59] The enhancement of EPC strength could be up to 20% according to the $E_{2g}$ peak shift from 570 $cm^{-1}$ (FS silicene) to 525 $cm^{-1}$ ($\sqrt{3}\times\sqrt{3}$ silicene).

In addition to the variation of the $E_{2g}$ peak, five distinct Raman peaks in the low frequency region (220-470 $cm^{-1}$) were observed in the $\sqrt{3}\times\sqrt{3}$ phase (Figure 5(a)). The intensities of these peaks show a strong dependence on the coverage of $\sqrt{3}\times\sqrt{3}$ phase, while their intensity ratios are almost the same regardless of the coverage. Thus, the origin of these five peaks should be the same and is ascribed to the edges.[47] For the honeycomb structure, there are two edge types, zigzag and armchair, as shown in Figure 5(c) and (d). In graphene, the armchair and zigzag edges inducing the intervalley and intravalley scattering of the quasiparticles in Dirac cones correspond to the Raman-active D and D′ peaks, respectively.[60,61] Due to the low-buckled structure of silicene, the structural symmetry is further reduced in contrast to planar graphene. Thus, more edge types are expected to exist in $\sqrt{3}\times\sqrt{3}$ silicene layers, leading to the presence of more edge-induced Raman peaks (denoted as $D_1$ to $D_5$).

After tremendous work on Raman spectra, this technique has come to be regarded as a powerful and convenient tool to identify the quality of silicene. A related application has been dedicated to monitoring the possible degeneration of silicene-based electric devices.[62] The stability of silicene in air has been investigated in detail by *ex-situ* Raman measurements. For multilayer silicene covered by an $Al_2O_3$ capping layer, only mild surface oxidation is identified after 24 h exposure in air.[46] *Ex-situ* Raman spectra of bilayer silicene as a function of exposure time were examined by Du *et al*.[56] The intensity of the $E_{2g}$ peak decreases with increasing exposure time, combined with an intensified signal of the $SiO_x$ peak. Importantly, the $E_{2g}$ peak survives in the

Raman spectra until the sample has been exposed to ambient air for more than 150 h. Moreover, preservation of the silicene–Ag interface during transfer and subsequent device fabrication has proved to be an effective method during the encapsulated delamination transfer process, where the Raman signals taken 7 days after transfer remain the same as for the freshly grown sample.[62] Thus, the Raman signatures obtained along with the interpretations provide a referential basis for further studies and for potential applications of epitaxial silicene.

**Germanene**

The FS germanene shares a similar lattice structure to that of FS silicene (Figure 2(a)), where the degree of buckling and bond lengths are 0.7 Å and 2.44 Å, respectively.[24] The electronic structure of FS germanene is predicted to feature an energy gap of 23 meV in addition to Dirac fermion characteristics due to the larger spin orbit coupling (SOC) strength,[24,63] altering its electronic structure to produce novel transport and optoelectronic properties. In the case of the phonon properties, the calculated $E_{2g}$ peak position is at around 290 $cm^{-1}$, as shown in Figure 6(b).[28] Furthermore, another peak located at 165 $cm^{-1}$ corresponds to the out-of-plane transverse optical (oTO) phonon branch at Γ, which is evoked by the larger buckling value compared to that of silicene.[28] Experimentally, germanene has been successfully fabricated on metallic and semiconducting substrates, including Au(111),[64-66] Pt(111),[67] Al(111),[68] Cu(111),[69] Sb(111),[70] and $MoS_2$,[71] as there is no bulk allotrope of FS germanene in nature. The superstructures are formed on the top of these substrates instead of 1 ×1 FS germanene, in which different buckling structures and phonon properties are expected. Only the Raman spectra of germanene on the Au(111) surface have been investigated, however, due to the short time since the experimental discovery of germanene in 2014.

There are several arrangements of Ge atoms on the Au(111) surface, and the Raman spectrum

plays a crucial role in the identification and confirmation of these structures. The first Ge layer displays a disordered structure, in which there is no Raman signal. Thus, the first layer is attributed to the formation of Ge-Au alloy, based on the absence of Ge-Ge covalent bonds that could contribute to the Raman results, as shown in Figure 7(a).[66] For the second layer, a rectangular superstructure emerges with two Raman peaks at 179 $cm^{-1}$ and 228 $cm^{-1}$, respectively. Based on the structural simulations, the high-resolution STM images identify this phase as $\sqrt{7}\times\sqrt{7}$ superstructure (in terms of $1\times1$ FS germanene), matching the $4\times2\sqrt{3}$ supercell of Au(111), as shown in Figure 6. This structural mode is further confirmed by calculations of the vibration density of states (vDOS), as shown in Figure 7(b), where the peaks located at 179 $cm^{-1}$ and 228 $cm^{-1}$ are correlated with the oTO and $E_{2g}$ modes, respectively.[66] The $E_{2g}$ peak position of the $\sqrt{7}\times\sqrt{7}$ superstructure is far away from those of FS germanene and Ge(111), which is a result of the large tensile strain and electron doping effect of the underlying Au(111) substrate. In fact, the average Ge-Ge bond length in the $\sqrt{7}\times\sqrt{7}$ superstructure is around 2.563 Å, giving a tensile strain of 4.91% compared to that of FS germanene (~2.443 Å ).[24,28,66] The $E_{2g}$ mode in FS germanene is softened by this biaxial tensile strain. Nevertheless, the oTO peak in the calculated result shows a weak dependence on the biaxial tensile strain, and its position is close to that in the experimental results. The Raman spectra for germanene on Au(111) display unique phonon modes distinct from those of Ge(111), which can be used as the Raman fingerprint to identify germanene on the Au(111) surface. Furthermore, since the in-plane Ge-Ge stretching mode ($E_{2g}$) could be defined as a characteristic phonon mode in EPC matrix elements, the shift of the $E_{2g}$ peak indicates enhancement of the EPC strength by up to 60%. Such an enlarged EPC is of particular interest because it gives rise to Kohn anomalies and superconductivity in the Bardeen−Cooper−Schrieffer superconductors,[10,72,73] raising the prospects for potential applications of this new 2D material.

## Conclusions and Outlook

The frequencies of vibration depend on the masses of the atoms involved and the strength of the bonds between them. In other words, more energy (a higher frequency) is required to vibrate a stronger bond, leading to low/high Raman shifts in heavy/light atoms and weak/strong bonds. Both the simulated and the experimental Raman results for graphene, silicene, and germanene follow this trend, as summarized in Table 1. Due to this relationship, Raman spectroscopy is typically used to show the presence of certain bonding types. Investigations of the vibrational properties of epitaxial silicene and germanene aim for a better understanding of the structural differences and for simplification of the seemingly complex phase diagrams. In addition to the typical $E_{2g}$ mode, the out-of-plane vibrational mode could be identified in both silicene and germanene due to their buckled structures, revealing the nature of the $sp^2$-$sp^3$ mixed state. The EPC strength of silicene and germanene has been successfully evaluated by analysis of their Raman spectra. The one-to-one relationship between various substrate-induced superstructures and their Raman fingerprints has been established after tremendous work, indicating that the Raman spectrum is an unambiguous, high-throughput, and nondestructive means to structural identification of these 2D materials. Moreover, the Raman spectrum has been used to monitor the air stability of silicene field-effect transistors operating at room temperature in practical application.

Nevertheless, the physical issues behind some of Raman peaks are still unclear. For example, no accurate relationship between the Raman peaks in silicene ($D_1$-$D_5$) and the zigzag and armchair edges has been established, requiring tip-enhanced Raman spectroscopy (TERS) to advance insights into the edge effects on phonon modes. Recently, new results for TERS with 0.5 nm spatial resolution have been achieved in silicene on Ag(111).[74] Due to the selective enhancement of Raman modes with vertical vibrational components in TERS, the vibrational properties of silicene phases,

which differ only in the bucking direction of the Si-Si bonds, could be identified. Studies of Raman spectra of silicene and germanene have only been performed on a few superstructures, which is far from adequate, due to their highly difficult fabrication (in ultra-high vacuum conditions). Considering the fact that various silicene and germanene reconstructions on different substrates have been investigated, further research on the Raman spectra for these reconstructions are expected, not only to detect more detailed vibrational information, but also to establish a general consensus between the buckled structures and the electronic properties of these 2D materials.

**Acknowledgements**

This work is supported by the Australian Research Council (ARC) through Discovery Projects (DP140102581, DP160102627 and DP170101467), the National Natural Science Foundation of China (Nos. 51472016, 51272015), and Fundamental Research Funds for the Central Universities (YWF-16-JCTD-B-03). The authors thank Dr. T. Silver for her valuable comments on this work.

**References**

1. Novoselov KS, Geim AK, Morozov SV *et al*. (2004) Electric field effect in atomically thin carbon films. *Science* **306(5696)**: 666-669.

2. Ferrari AC, Meyer JC, Scardaci V *et al*. (2006) Raman spectrum of graphene and graphene layers. *Physical Review Letters* **97(18)**: 187401.

3. Basko DM, Aleiner IL (2008) Interplay of Coulomb and electron-phonon interactions in graphene. *Physical Review B* **77(4)**: 041409.

4. Bonini N, Lazzeri N, Marzari N *et al*. (2007) Phonon anharmonicities in graphite and graphene. *Physical Review Letters* **99 (17)**: 176802.

5. Ferrari AC (2007) Raman spectroscopy of graphene and graphite: Disorder, electron-phonon

coupling, doping and nonadiabatic effects. *Solid State Communications* **143(1-2)**: 47-57.

6. Kalbac M, Reina-Cecco A, Farhat H *et al*. (2010) The influence of strong electron and hole doping on the Raman intensity of chemical vapor-deposition graphene. *ACS Nano* **4(10)**: 6055-6063.

7. Chen CF, Park CH, Boudouris BW *et al*. (2011) Controlling inelastic light scattering quantum pathways in graphene. *Nature* **471(7340)**: 617-620.

8. Das A, Pisana S, Chakraborty B *et al*. (2008) Monitoring dopants by Raman scattering in an electrochemically top-gated graphene transistor. *Nature Nanotechnology* **3(4)**: 210-215.

9. Zhao WJ, Tan PH, Liu J *et al*. (2011) Intercalation of few-layer graphite flakes with $FeCl_3$: Raman determination of Fermi level, layer by layer decoupling, and stability. *Journal of the American Chemical Society* **133(15)**: 5941-5946.

10. Yan J, Zhang YB, Kim P *et al*. (2007) Electric field effect tuning of electron-phonon coupling in graphene. *Physical Review Letters* **98(16)**: 166802.

11. Huang M, Hugen Y, Heinz TF *et al*. (2010) Probing strain induced electronic structure change in graphene by Raman spectroscopy. *Nano Letters* **10(10)**: 4074-4079.

12. Mohr M, Maultzsch J and Thomsen C (2010) Splitting of the Raman 2D band of graphene subjected to strain. *Physical Review B* **82(20)**: 201409.

13. Yoon D, Son YW and Cheong H (2011) Strain-dependent splitting of double resonance Raman scattering band in graphene. *Physical Review Letters* **106(15)**: 155502.

14. Mohiuddin TMG, Lombardo A, Nair RR *et al*. (2009) Uniaxial strain in graphene by Raman spectroscopy: G peak splitting, Gruneisen parameters, and sample orientation. *Physical Review B* **79(20)**: 205433.

15. Ni ZH, Yu T, Lu YH *et al*. (2008) Uniaxial strain on graphene: Raman spectroscopy study and

band-gap opening. *ACS Nano* **2(11)**: 2301-2305.

16. Cançado LG, Jorio A, Ferreira EHM *et al*. (2011) Quantifying defects in graphene via Raman spectroscopy at different excitation energies. *Nano Letters* **11(8)**: 3190-3196.

17. Faugeras C, Amado M, Kossacki P *et al*. (2009) Tuning the electron-phonon coupling in multilayer graphene with magnetic fields. *Physical Review Letters* **103(18)**: 186803.

18. Faugeras C, Amado M, Kossacki P *et al*. (2011) Magneto-Raman scattering of graphene on graphite: Electronic excitations and their coupling to optical phonons. *Physical Review Letters* **107(3)**: 036807.

19. Ferrari AC and Robertson J (2000) Interpretation of Raman spectra of disordered and amorphous carbon. *Physical Review B* **61(20)**: 14095-14107.

20. Thomsen C and Reich S (2000) Double resonant Raman scattering in graphite. *Physical Review Letters* **85(24)**: 5214-5217.

21. You Y, Ni Z, Yu T *et al*. (2008) Edge chirality determination of graphene by Raman spectroscopy. *Applied Physics Letters* **93(16)**: 163112.

22. Casiraghi C, Hartschuh A, Qian H *et al*. (2009) Raman spectroscopy of graphene edges. *Nano Letters* **9(4)**: 1433-1441.

23. Tan PH, Pan WP, Zhao WJ *et al*. (2012) The shear mode of multilayer graphene. *Nature Materials* **11(4)**: 294-300.

24. Liu CC, Feng W and Yao Y (2011) Quantum spin Hall effect in silicene and two-dimensional germanium. *Physical Review Letters* **107(7)**: 076802.

25. Zhao JJ, Liu HS, Yu ZM *et al*. (2016) Rise of silicene: A competitive 2D material. *Progress in Materials Science* **83**: 24-151.

26. Vogt P, De Padova P, Quaresima C *et al*. (2012) Silicene: Compelling experimental evidence for

graphenelike two-dimensional silicon. *Physical Review Letters* **108(15)**: 155501.

27. Li L, Lu S, Pan J *et al*. (2014) Buckled germanene formation on Pt(111). *Advanced Materials* **26(28)**: 4820-4824.

28. Scalise E, Houssa M, Geoffrey R *et al*. (2013) Vibrational properties of silicene and germanene. *Nano Research* **6(1)**: 19-28.

29. Yan J, Stein R, Schaefer DM *et al*. (2013) Electron-phonon coupling in two-dimensional silicene and germanene. *Physical Review B* **88(12)**: 121403.

30. Parker JH, Feldman DW and Ashkin M. (1967) Raman scattering by silicon and germanium. *Physical Review* **155(3)**: 712-714.

31. Scalise E, Cinquanta E, Houssa M *et al*. (2014) Vibrational properties of epitaxial silicene layers on (111) Ag. *Applied Surface Science* **291**: 113-117.

32. Feng B, Ding Z, Meng S *et al*. (2012) Evidence of silicene in honeycomb structures of silicon on Ag(111). *Nano Letters* **12(7)**: 3507-3511.

33. Chen L, Liu CC, Feng B *et al*. (2012) Evidence for Dirac fermions in a honeycomb lattice based on silicon. *Physical Review Letters* **109(5)**: 056804.

34. De Padova P, Vogt P, Resta A *et al*. (2013) Evidence of Dirac fermions in multilayer silicene. *Applied Physics Letters* **102(16)**: 163106.

35. Chen L, Li H, Feng B *et al*. (2013) Spontaneous symmetry breaking and dynamic phase transition in monolayer silicene. *Physical Review Letters* **110(8)**: 085504.

36. Du Y, Zhuang JC, Liu H *et al*. (2014) Tuning the band gap in silicene by oxidation. *ACS Nano* **8(10)**: 10019-10025.

37. Xu X, Zhuang JC, Du Y *et al*. (2014) Effects of oxygen adsorption on the surface state of epitaxial silicene on Ag(111). *Scientific Reports* **4**: 7543.

38. Zhuang JC, Xu X, Feng HF *et al*. (2015) Honeycomb silicon: A review of silicene. *Science Bulletin* **60(18)**: 1551-1562.

39. Liu ZL, Wang MX, Xu JP *et al*. (2014) Various atomic structures of monolayer silicene fabricated on Ag(111). *New Journal of Physics* **16**: 075006.

40. Meng L, Wang Y, Zhang L *et al*. (2013) Buckled silicene formation on Ir(111). *Nano Letters* **13(2)**: 685-690.

41. Huang L, Zhang YF, Zhang YY *et al*. (2017) Sequence of silicon monolayer structures grown on a Ru surface: From a herringbone structure to silicene. *Nano Letters* **17(2)**: 1161-1166.

42. Fleurence A, Friedlein R, Ozaki T *et al*. (2012) Experimental evidence for epitaxial silicene on diboride thin films. *Physical Review Letters* **108(24)**: 245501.

43. Chiappe D, Scalise E, Cinquanta E *et al*. (2014) Two-Dimensional Si Nanosheets with Local Hexagonal Structure on a $MoS_2$ Surface. *Advanced Materials* **26(13)**: 2096-2101.

44. Volders C, Monazami E, Ramalingam G *et al*. (2017) Alternative route to silicene synthesis via surface reconstruction on *h*‾ $MoSi_2$ crystallites. *Nano Letters* **17(1)**: 299-307.

45. Noguchi E, Sugawara K, Yaokawa R *et al*. (2015) Direct observation of Dirac cone in multilayer silicene intercalation compound $CaSi_2$. *Advanced Materials* **27(5)**: 856-860.

46. Cinquanta E, Scalise E, Chiappe D *et al*. (2013) Getting through the nature of silicene: An $sp^2$-$sp^3$ two-dimensional silicon nanosheet. *The Journal of Physical Chemistry C* **117(32)**: 16719-16724.

47. Zhuang JC, Xu X, Du Y *et al*. (2015) Investigation of electron-phonon coupling in epitaxial silicene by *in situ* Raman spectroscopy. *Physical Review B* **91(16)**: 161409.

48. Iqbal Z and Vepřek S (1982) Raman scattering from hydrogenated microcrystalline and amorphous silicon. *Journal of Physics C: Solid State Physics* **15(2)**: 377-392.

49. Li BB, Yu DP and Zhang SL (1999) Raman spectral study of silicon nanowires. *Physical Review B* **59(3)**: 1645-1648.

50. D áz Álvarez A, Zhu T, Nys JP *et al*. (2016) Scanning tunnelling spectroscopy and Raman spectroscopy of monolayer silicene on Ag(111). *Surface Science* **653**: 92-96.

51. Solonenko D, Gordan OD, Le Lay G *et al*. (2016) 2D vibrational properties of epitaxial silicene on Ag(111). *2D Materials* **4(1)**: 015008.

52. Solonenko D, Gordan OD, Le Lay G *et al*. (2017) Comprehensive Raman study of epitaxial silicene-related phases on Ag(111). *Beilstein Journal of Nanotechnology* **8:** 1357-1365.

53. Tsoutsou D, Xenogiannopoulou E, Golias E *et al*. (2013) Evidence for hybrid surface metallic band in (4×4) silicene on Ag(111). *Applied Physics Letters* **103(23)**: 231604.

54. Avila J, De Padova P, Cho S *et al*. (2013) Presence of gapped silicene-derived band in the prototypical (3×3) silicene phase on silver (111) surfaces. *Journal of Physics: Condensed Matter* **25(26)**: 262001.

55. De Padova P, Avila J, Resta A *et al*. (2013) The quasiparticle band dispersion in epitaxial multilayer silicene. *Journal of Physics: Condensed Matter* **25(38)**: 382202.

56. Du Y, Zhuang JC, Wang JO *et al*. (2016) Quasi-freestanding epitaxial silicene on Ag(111) by oxygen intercalation. *Science Advances* **2(7)**: e1600067.

57. Zhuang JC, Xu X, Peleckis G *et al*. (2017) Silicene: A promising anode for lithium-ion batteries. *Advanced Materials* doi: 10.1002/adma.201606716.

58. Li Z, Zhuang JC, Chen L *et al*. (2016) Observation of van Hove singularities in twisted silicene multilayers. *ACS Central Science* **2(8)**: 517-521.

59. Si C, Liu Z, Duan WH *et al*. (2013) First-principles calculations on the effect of doping and biaxial tensile strain on electron-phonon coupling in graphene. *Physical Review Letters* **111(19)**:

196802.

60. Cançado LG, Pimenta MA, Neves BRA *et al*. (2004) Influence of the atomic structure on the Raman spectra of graphite edges. *Physical Review Letters* **93(24)**: 247401.

61. Saito R, Dresselhaus G and Dresselhaus MS (2000) Trigonal warping effect of carbon nanotubes. *Physical Review B* **61(4)**: 2981-2990.

62. Tao L, Cinquanta E, Chiappe D *et al*. (2015) Silicene field-effect transistors operating at room temperature. *Nature Nanotechnology* **10(3)**: 227-231.

63. Liu CC, Jiang H and Yao Y. (2011) Low-energy effective Hamiltonian involving spin-orbit coupling in silicene and two-dimensional germanium and tin. *Physical Review B* **84(19)**: 195430.

64. Dávila ME, Xian L, Cahangirov S *et al*. (2014) Germanene: A novel two-dimensional germanium allotrope akin to graphene and silicene. *New Journal of Physics* **16(9)**: 095002.

65. Dávila ME and Le Lay G (2016) Few layer epitaxial germanene: A novel two-dimensional Dirac material. *Scientific Reports* **6**: 20714.

66. Zhuang JC, Gao N, Li Z *et al*. Cooperative electron-phonon coupling and buckled structure in germanene on Au(111). *ACS Nano* **11(4)**: 3553-3559.

67. Li L, Lu S, Pan J *et al*. (2014) Buckled germanene formation on Pt(111). *Advanced Materials* **26(28)**: 4820-4824.

68. Derivaz M, Dentel D, Stephan R *et al*. (2015) Continuous germanene layer on Al(111). *Nano Letters* **15(4)**: 2510-2516.

69. Qin Z, Pan J, Lu S *et al*. (2017) Direct evidence of Dirac signature in bilayer germanene islands on Cu(111). *Advanced Materials* **29(13)**: 1606046.

70. Gou J, Zhong Q, Sheng S *et al*. (2016) Strained monolayer germanene with 1×1 lattice on Sb(111). *2D Materials* **3(4)**: 045005.

71. Zhang L, Bampoulis P, Rudenko AN *et al*. Structural and Electronic Properties of Germanene on $MoS_2$. *Physical Review Letters* **116(25)**: 256804.

72. Si C, Liu Z, Duan WH *et al*. (2013) First-principles calculations on the effect of doping and biaxial tensile strain on electron-phonon coupling in graphene. *Physical Review Letters* **111(19)**: 196802.

73. Piscanec S, Lazzeri M, Mauri F *et al*. (2004) Kohn anomalies and electron-phonon interactions in graphite. *Physical Review Letters* **93(18)**: 185503.

74. Sheng S, Wu J, Cong X *et al*. (2017) Vibrational properties of a monolayer silicene sheet studied by tip-enhanced Raman spectroscopy. *Physical Review Letters* **Accepted.**

75. Slonczewski JC and Weiss PR (1958) Band structure of graphite. *Physical Review* **109(2):**272.

76. Yao Y, Ye F, Qi X *et al*. (2007) Spin-orbit gap of graphene: First-principles calculations. *Physical Review B* **75(4)**: 041401

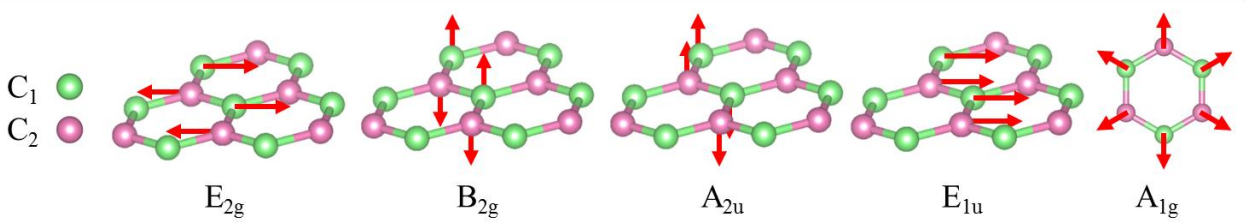


Figure 1 Γ and K point phonon-displacement pattern for graphene. $E_{2g}$, $B_{2g}$, $A_{2u}$, and $E_{1u}$ are vibrational modes at the Γ point, and $A_{1g}$ mode is from the K point. Green and pink balls represent inequivalent carbon atoms. Red arrows show atom displacements.

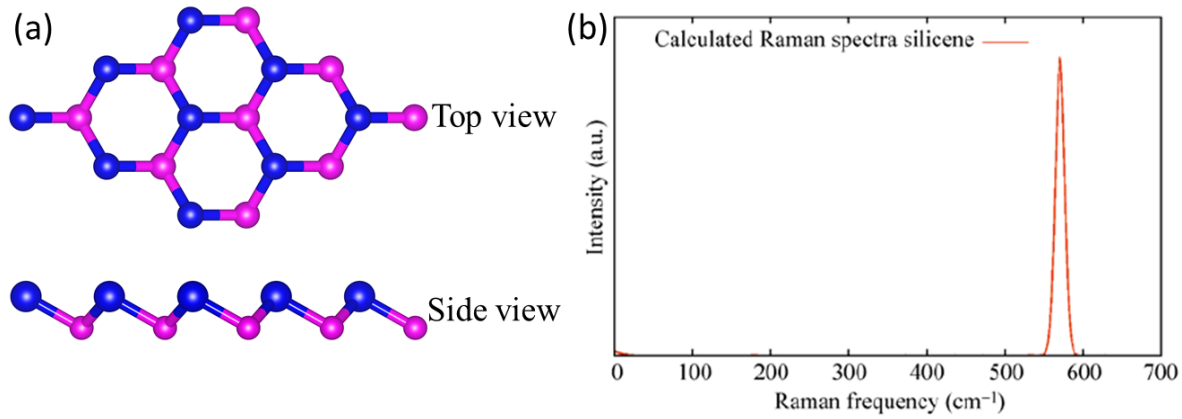


Figure 2 (a) Top and side views of the buckled honeycomb arrangement of predicted free-standing silicene and germanene. The blue and pink balls represent buckled-up and buckled-down atoms, respectively. (b) Simulated Raman spectrum of free-standing silicene.[28]

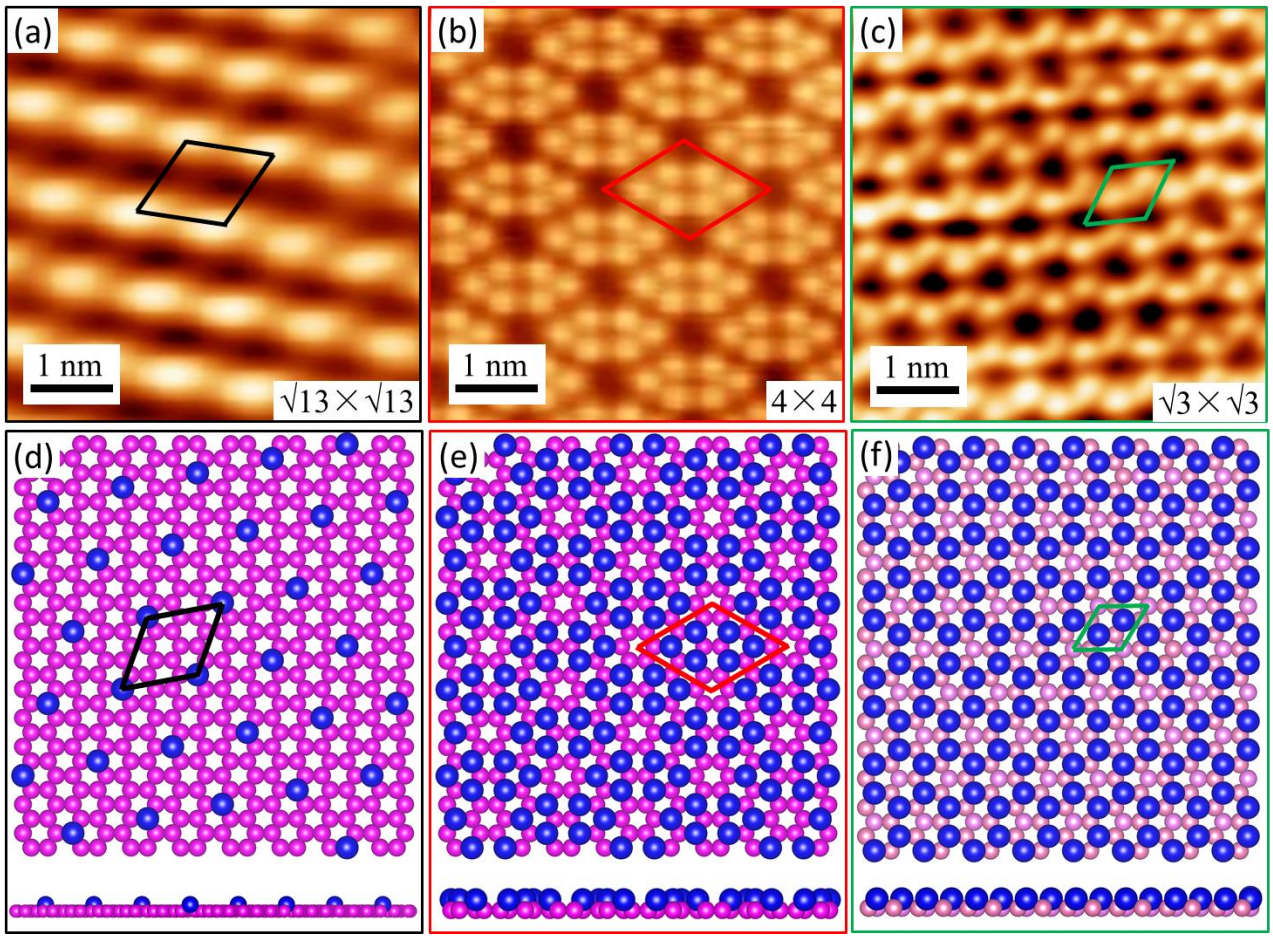


Figure 3 Multiple superstructures of silicene on Ag(111) substrate. High-resolution STM images of (a) √13×√13 phase (5 nm × 5 nm, $V_s$ = -0.4 V, $I_t$ = 3 nA), (b) 4×4 phase (5 nm × 5 nm, $V_s$ = 30 mV, $I_t$ = 4 nA), and (c) √3×√3 silicene (5 nm × 5 nm, $V_s$ = 0.5 V, $I_t$ = 4 nA).[44] (c)-(e) Correlated illustrations of silicene in various phases for both top view and side view, in which the blue and pink balls represent top-layer and bottom-layer Si atoms, respectively. The black rhombus in (d), red rhombus in (e), and green rhombus in (f) stand for the unit cell of √13×√13 phase, 4×4 phase, and √3×√3 phase, respectively.

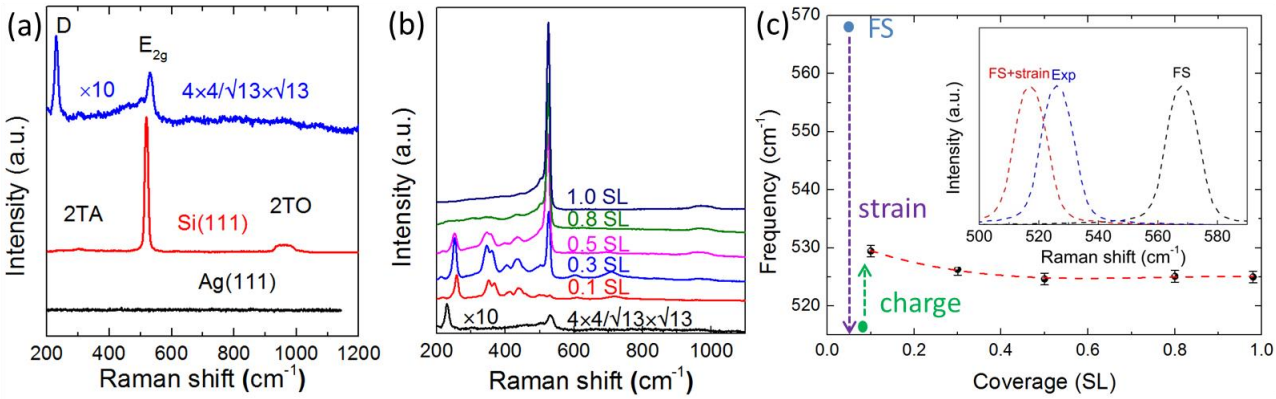


Figure 4 (a) Raman spectrum of the √13×√13/4×4 mixed phase. The Ag(111) substrate and Si(111) are displayed as the references.[47] (b) Raman spectra of √3×√3 silicene grown on a √13×√13/4×4 initial layer with different coverage. The intensity value of the √13×√13/4×4 spectrum is enlarged by 10 times as a guide for comparison with the Raman spectra of √3×√3 silicene. "SL" denotes the coverage of the √3×√3 silicene layer.[47] (c) The peak position of the $E_{2g}$ mode is dependent on the coverage. The inset of (c) is a sketch to illustrate the combined effects of strain and doping on the $E_{2g}$ peak frequency.[47]

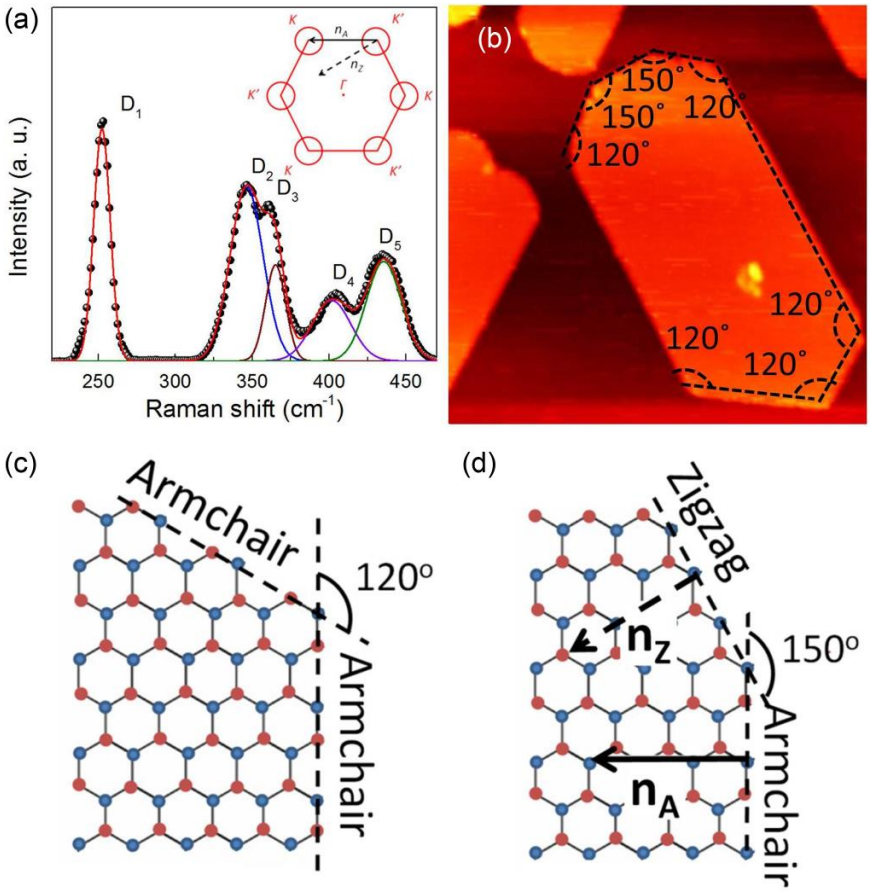


Figure 5 (a) Raman spectrum of $\sqrt{3}\times\sqrt{3}$ silicene layers with the fitted results in the frequency range of 220-470 $cm^{-1}$, from which the peaks could be identified and are marked as $D_1$-$D_5$.[47] (b) STM image of $\sqrt{3}\times\sqrt{3}$ silicene with two typical edge arrangements: armchair/zigzag and armchair/armchair, corresponding to two edge angles of 150 ° and 120 °, respectively.[47] (c), (d) Schematic diagram of atomic structures of armchair and zigzag edges. Only the armchair edge connects two different valleys in the Brillouin zone, as illustrated in the inset of (a).[47]

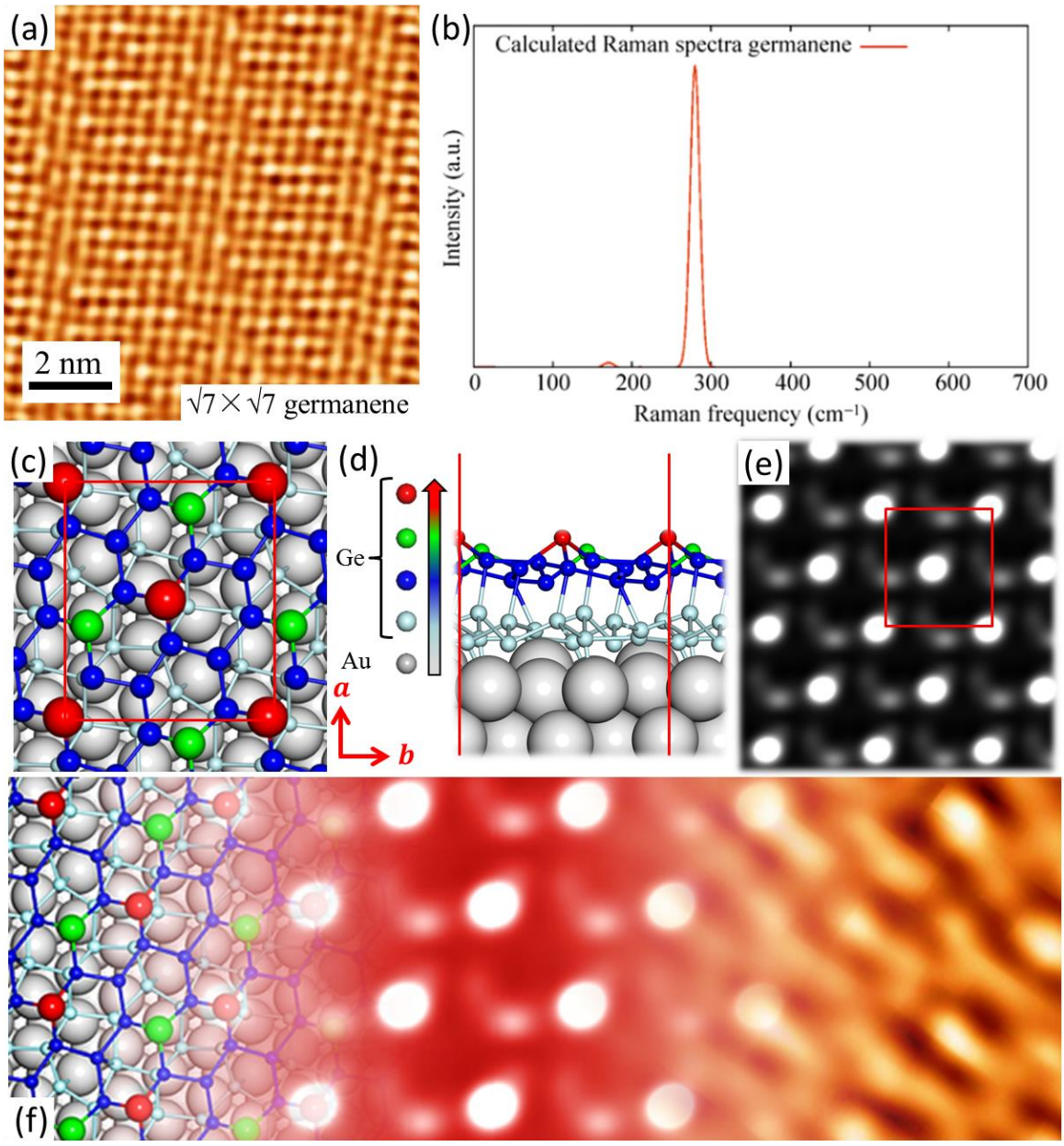


Figure 6 (a) STM image of √7×√7 germanene on Au(111) substrate (10 nm × 10 nm, $V_s$ = 20 mV, $I_t$ = 50 pA).[66] (b) Simulated Raman spectra of free-standing germanene.[28] Top (c) and side (d) views of the relaxed model of the atomic structure of the √7×√7 germanene, corresponding to the 4×2√3 unit cell of the Au(111) configuration. The red rectangle represents the unit cell of √7×√7 germanene. The vectors *a* and *b* represent lattice directions. Δ*z* stands for the degree of buckling of the √7 ×√7 germanene.[66] (e) Simulated STM image of √7×√7 germanene based on the model in (c) and (d). (f) Juxtaposition of the relaxed model of the atomic structure, the simulated STM image,

and the experimental STM image (from left to right).[66]

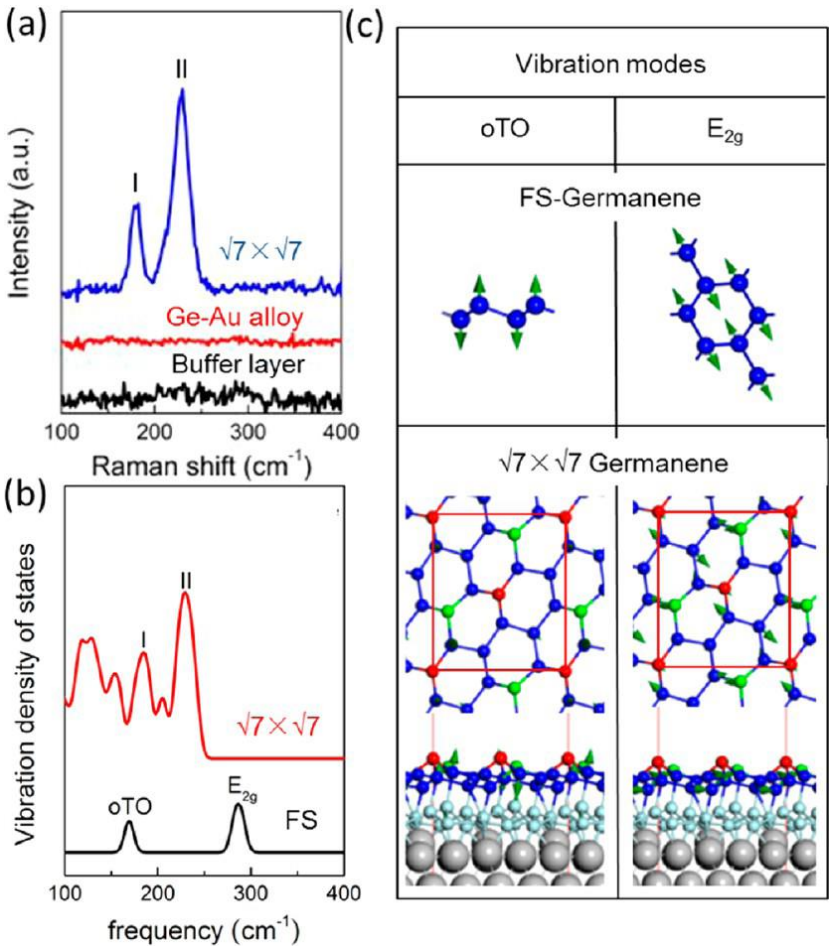


Figure 7 (a) Raman spectrum of √7×√7 germanene phase. The Raman results for the buffer layer (first layer) and Ge-Au alloy are included as references.[61] (b) Density functional theory simulations of the vibration density of states of both free-standing germanene and √7×√7 germanene on Au(111).[66] (c) Comparative calculations of the vibration modes for both the free-standing germanene and the √7×√7 germanene/4×2√3 Au(111) configurations from the dynamical matrix.[66]

Table 1 Detailed structural parameters and Raman peak positions of graphene, silicene, and germanene: bond length ($d_B$), buckling height ($H_B$), lattice constant ($a$), peak frequencies of the $E_{2g}$ and oTO modes for both the free-standing predictions (FS) and the experimental results (EXP), and the energy gap (Δ).

| **Type** | $d_B$ **(Å)** | $H_B$ **(Å)** | $a$ **(Å)** | $E_{2g}$ **(cm$^{-1}$)** | | **oTO (cm$^{-1}$)** | | Δ **(meV)** |
|---|---|---|---|---|---|---|---|---|
| | | | | **FS** | **EXP** | **FS** | **EXP** | |
| **Graphene** | 1.42[75] | 0[75] | 2.46[75] | 1600[28] | 1580[2] | n/a | n/a | ~0[10,76] |
| **Silicene** | 2.32~2.38[24,28] | 0.44[28] | 3.86[24] | 570[28] | 530[47] | 180[28] | 230[44] | 1.55[24] |
| **Germanene** | 2.42[24] | 0.7[28] | 3.97~4.02[24,28] | 290[28] | 228[66] | 165[28] | 179[66] | 23.9[24] |